WAFER-SCALE LASER LITHOGRAPHY: I. PYROLYTIC DEPOSITION OF METAL MICROSTRUCTURES*

IRVING P. HERMAN, RODERICK A. HYDE, BRUCE M. MCWILLIAMS, ANDREW H. WEISBERG and LOWELL L. WOOD.

Physics Department, Lawrence Livermore National Laboratory, P.O. Box 808-L-278, Livermore, CA 94550

ABSTRACT

Mechanisms for laser-driven pyrolytic deposition of micron-scale metal structures on crystalline silicon have been studied. Models have been developed to predict temporal and spatial properties of laser-induced pyrolytic deposition processes. An argon ion laser-based apparatus has been used to deposit metal by pyrolytic decomposition of metal alkyl and carbonyl compounds, in order to evaluate the models. These results of these studies are discussed, along with their implications for the high-speed creation of micron-scale metal structures in ULSI systems.

INTRODUCTION

In order that state-of-the-art computers can reproduce with less human interference and thus with lower error rates and latencies, it is necessary for them to be able to micropattern semiconductor substrates directly and at high speed. Contemporary supercomputer systems composed of 10^8 transistors, each constituted of as many as 10^2 'tiles' of various materials stacked in particular arrangements, contain as many as 10^{10} 'tiles' in their ultra-large scale integrated (ULSI) patterns. In order that latencies involved in computer-directed generation of new computer-scale micropatterns be not much greater than a day, creation of a single 'tile' must be accomplished in an interval of the order of 10^{-5} seconds.

In the series of papers of which this is the first, we will report on means for accomplishing such processing in this context. This paper reports on that aspect of laser micropatterning which is possibly the least advanced through the present: the discretionary, high-speed generation of lines of metal—paths of metallic 'tiles' laid edge-to-edge—suitable for interconnecting active devices in ULSI circuits.

Monolithically implemented computers of the present era consist of sheets of metal traces of micron-scale width and thickness, separated almost (but not quite) everywhere from each other by nearly hole-free dielectric sheets, and occasionally touching the terminals of transistor devices which are embedded for convenience in a semiconductor substrate common to all such devices. The large majority of the structure (indexed by the fraction of total 'tiles' in the pattern) of computers implemented in the ever more popular metal-oxide semiconductor (MOS) family of technologies is expressed in metal (or in surrogate metal, highly doped polysilicon). It is thus quite crucial to greatly extend the hitherto highly limited ability to create suitable metal microstructures directly with laser processing techniques, as this approach is qualitatively superior to all other current

* Work performed under the auspices of the U.S. Department of Energy by the Lawrence Livermore National Laboratory under contract number W-7405-ENG-48.

Mat. Res. Soc. Symp. Proc. Vol. 17 (1983)

prospects for high-speed, computer-controlled micropattern generation directly on semiconductor substrates.

We report here an order of magnitude enhancement in the rate of metal micropatterning in the ULSI context, relative to the highest rates previously reported. Taken together with results from other workers on rapid semiconductor substrate doping and dielectric layer creation, this advance makes feasible in principle the generation of monolithic, ULSI supercomputers on day time scales.

The laser-driven metal deposition processes of interest consist of a semiconductor substrate surfaced with the reactant gas, with a laser beam focused to the region on the substrate where metal is to be deposited. Two different types of laser-induced metal deposition processes are candidates for this role: pyrolysis and photolysis. The pyrolytic processes are based on thermal decomposition reactions which occur due to laser-induced heating of the substrate, while the photolytic processes entail gas phase photolytic decomposition reactions occurring in the laser-irradiated gas-filled region above the substrate.

The ultimate limit on the rate of metal deposition by either pyrolytic or photolytic processes is determined by the maximum possible rate of mass transport of the reactant gas to the substrate. Pyrolytic processes may usefully be thought of as unimolecular decompositions, while photolytic ones are two-body (binary) ones in the same sense—both gas molecules and photons must occupy the same space-time volume for photolysis to occur.

In order for photolysis to occur in unit time, the photon fluence must equal the reciprocal of the cross-section for the metal-bearing molecule to photolytically absorb the photon. Since the unit of time is that for the molecule to transit the reaction zone—about 10 nanoseconds for molecular weights of the order of 100 amu and reaction zone scales of the order of 1 micron—and since the largest photolytic cross-sections of interest less than 10^{-17} cm^2, the photon fluxes required for mass transport-limited photolysis are of the order of 10^{25} photons cm^{-2} sec^{-1}, or about 10 megawatt cm^{-2}, which implies a minimum input of 0.1 watts of hard-won 4-6 eV laser photons.

By way of comparison, the laser intensity required for pyrolysis of metal-bearing gases of interest at a comparable mass-processing rate is just that needed to maintain a square micron of substrate at a temperature of the order of 1000°K, which is again about 10^7 watts cm^{-2}, but now involves an input of 0.1 watts of readily available, wavelength-insensitive optical laser spectral power. Thus, even when using metal-bearing gases with the highest UV photolytic cross-sections, the laser intensity regime for efficient photolysis already completely overlaps the one for pyrolysis, but is accessed with substantially greater technical difficulty. When using gases with more typical photolytic cross-sections, the laser intensities required for efficient photolysis will boil the substrate on nanosecond time scales. Intensity reduction to more acceptable levels will slow the photolysis rate, relative to the photolytic one, by the ratio of the photolytic cross-section to the peak value of 10^{-17} cm^2, e.g., for aluminum trimethyl with its photolytic cross-section of 10^{-20} cm^{-2}($\lambda \simeq 0.26\ \mu m$), photolytic deposition of aluminum metal will be approximately three orders of magnitude slower than will pyrolytic.

We therefore restrict our attention to pyrolytic mechanisms of metal micropatterning of semiconductor substrates. Earlier work has demonstrated photolytic deposition of Al, Cd, Zn and Sn from gas-phase and surface decomposition of the respective alkyls[R1], and of Fe, W, Cr, and Mo from the respective carbonyls[R2,R3], using ultraviolet ($\lambda \leq 0.26\ \mu m$) laser light. Previous workers have pyrolytically deposited large, dendrite-rich strips of Al, Zn and Cd at low speeds on GaAs surfaces with focussed radiation from a krypton-ion laser[R4], and deposited large scale Ni[R5] and W[R6] films with CO_2 laser radiation focused on silica surfaces.

Mass transport-limited, laser-driven pyrolysis of dimethyl zinc, trimethyl aluminum and nickel carbonyl to form metal traces with micron-scale widths and thicknesses on

silicon wafers by focused argon-ion laser light ($\lambda = 0.5145\ \mu m$) is reported in the present paper. Because of its superior properties—high $Ni(CO)_4$ vapor pressure, high melting point, high electrical conductivity and excellent corrosion resistance of metallic nickel, and good model qualities for other systems of interest—this nickel system has been singled out for extensive study. We interpret these results with theories of quantitative predictive quality, and thereby extrapolate them to ULSI applications of ultimate interest.

THEORY OF LASER-INDUCED PYROLYTIC DEPOSITION PROCESSES

The laser-induced pyrolytic metal deposition processes under consideration are based on thermal decomposition reactions of the form:

$$[MX_n] \rightarrow [M] + n[X] \tag{1}$$

where MX_n is the reactant gas molecule (*e.g.*, a metal alkyl or carbonyl), M is the metal atom being deposited, and X is a product gas of the reaction. The process can be thought of as involving five consecutive steps:

a. Diffusion of the reactant gas to the heated portion of the substrate;
b. Adsorption of reactant;
c. Decomposition of the reactant;
d. Desorption of the volatile product; and
e. Diffusion of the product gas away from the substrate.

At lower temperatures, the rate-determining step of the process is usually (c); at higher temperatures, where the decomposition reaction rate becomes substantial, (a) and (e) become the rate-limiting steps.

We present a generally applicable model for high-speed deposition of metal microstructures by pyrolysis of a metal-bearing gas, emphasizing generation of micron-scale nickel traces by pyrolysis of $Ni(CO)_4$.

The kinetics of processes (b) through (d) have been analyzed by Carlton and Oxley[R7]. Their expression for the overall reaction rate is:

$$R(p_1, p_2, T) = R_0(T) f(p_1, p_2, T) \tag{2}$$

where

$$R_0(T) = 5.1 \times 10^{29} exp\{-T_0/T\} \quad cm^{-2} sec^{-1}; \quad T_0 = 11,022°K \tag{3}$$

$$f(p_1, p_2, T) = k_1^2 [p_1^2 - (p_2^4/K_{eq})^2]/[1 + k_1 p_1 + k_2 p_2]^2 \tag{4}$$

$$\begin{aligned} k_1 &= 0.089 exp\{T_1/T\} \quad Torr^{-1}; \quad T_1 = 352°K \\ k_2 &= 0.00152 exp\{T_2/T\} \quad Torr^{-1}; \quad T_2 = 2,013°K \\ K_{eq} &= 1.4 \times 10^{31} exp\{-T_3/T\} \quad Torr^2; \quad T_3 = 18,800°K \quad [R8] \end{aligned} \tag{5}$$

Here p_1 is the $Ni(CO)_4$ partial pressure, while p_2 is that of CO. The reaction is second order and is choked at high pressure by adsorbed $Ni(CO)_4$ and CO. Since f is always less than one, R_0 represents the peak rate possible, which is attained at high p_1 and low p_2. We can neglect the reverse reaction, since at the temperatures needed to make R_0 large, the equilibrium constant for the reaction, K_{eq}, is also large; the recombination reaction is thus negligible for present purposes.

Examination of (2) shows that, as we increase surface temperature, the rate will climb due to the activation energy factor R_0. Eventually, though, we will reach an asymptotic condition where gas diffusion is insufficient either to maintain p_1 near its far-field value, or to disperse CO and keep p_2 low near the deposition site. Both of these effects will cause f to fall. Our model must therefore relate T to laser power, and must consider gas diffusive mass transport. First we obtain $R_0(T)$.

The temperature field produced in a plane slab of solid silicon by a linearly swept laser beam of Gaussian profile has been treated previously[R9, R10]. Using a Kirchhoff transform we define a linearized temperature:

$$\theta(T) = \int_{T_r}^{T} \frac{K(T')}{K(T_r)} dT', \tag{6}$$

where T_r is the reference (initial) temperature. Writing the space- and time-dependent laser intensity I as

$$I(x - vt, y) = \frac{P}{\pi r_0^2} exp\left\{-\frac{(x - vt)^2 + y^2}{r_0^2}\right\} \tag{7}$$

where P is the incident laser power and v s the laser focal spot sweep rate, then

$$\theta(X, Y, Z; V) = \frac{2}{\pi}\theta_c \int_0^{\infty} exp\left\{-\frac{(X + Vu^2)^2 + Y^2}{1 + u^2} - \frac{Z^2}{u^2}\right\} \frac{du}{1 + u^2} \tag{8}$$

where

$$X = \frac{x}{r_0} \qquad Y = \frac{y}{r_0} \qquad Z = \frac{z}{r_0} \qquad V = \frac{vr_0}{\sqrt{8D}} \tag{9}$$

$$\theta_c = \frac{P(1 - \Re_S)}{2\sqrt{\pi} K(T_r) r_0} \tag{10}$$

This temperature solution is found via a Green's function route. This approach is not exactly correct, since the silicon thermal diffusivity D is temperature-dependent, but for "relatively slow" scan velocities, D fades from significance.

The reflectivity $\Re_S$ has been assumed constant over the laser beam focal spot, which is reasonable for solid Si. The term θ_c is the peak value of θ for the static case; to relate it to the actual temperature, we must assume an expression for thermal conductivity. We use $K(T)$ and $\Re_S$ from[R9]:

$$K(T) = \frac{k}{T - T_k}; \qquad k = 299\ W/cm; \qquad T_k = 99°K \tag{11}$$

$$\Re_S(T) = 0.367 + 4.29 \times 10^{-5} T$$

Solving (6) gives

$$\theta(T) = (T_r - T_k) ln \frac{T - T_k}{T_r - T_k}. \tag{12}$$

$$T(\theta) = T_k + (T_r - T_k) exp\left\{\frac{\theta}{T_r - T_k}\right\} \tag{13}$$

$$T_c = T_k + (T_r - T_k) exp\left\{\frac{P(1 - \Re_S)}{2\sqrt{\pi} k r_0}\right\} \tag{14}$$

For $P = 300$ mW and $r_0 = 2\ \mu m$, we find $T_c = 575°$K.

The simplest expression for metal deposition rate is obtained by assuming a relatively slow laser focal spot scan rate and looking at the center of the spot; placing (14) in rate

(3) we obtain the rate of increase of the metal film thickness $\dot{W}_c$:

$$\dot{W}_c = 5.6 \times 10^{10} exp\{-T_0/T_c\} \quad \mu m/sec \tag{15}$$

This is plotted in Figure 1 as a function of specific laser power P/r_0, using $T_r = 300°K$. This model can also predict the spatial variation of growth rate by combining (3), (8) and (13). We can obtain a simple relation by Taylor expansion, which is useful since $T << T_0$

$$\theta(r) \approx \theta_c[1 - \frac{r^2}{2r_0^2}] \tag{16}$$

$$T(r) \approx T_c - \theta_c \frac{T_c - T_k}{T_r - T_k} \frac{r^2}{2r_0^2} \tag{17}$$

so

$$\dot{W} \approx \dot{W}_c exp\{-r^2/\rho^2\} \tag{18}$$

where ρ is the effective interaction radius

$$\frac{\rho}{r_0} = \frac{T_c}{\sqrt{T_0 \theta_c}} \sqrt{2 \frac{T_r - T_k}{T_c - T_k}} \tag{19}$$

For example, at $P/r_0 = 0.15\ W/\mu m$, we find $\rho/r_0 = 0.38$, so the Ni spot size should be about 2.5 times smaller than that of the laser.

The growth rates of Figure 1, based on Equation 15, are invalid at high temperatures, because gas diffusion cannot supply $Ni(CO)_4$ or remove CO sufficiently rapidly. Therefore, we need to obtain $f(p_1, p_2, T)$ and do so by analyzing gas diffusion by a Green's function approach analogous to (8). Solving for the "relatively slow" scan case using a reaction rate spatial variation as in (18), the species population changes at spot center are

$$\Delta n_i = \frac{\sqrt{\pi}}{2} \rho \frac{R_i}{D_i} \quad cm^{-3}; \quad i = 1, 2 \tag{20}$$

Here the rate for $Ni(CO)_4$, R_1, is $-R$ from (2), while R_2 for CO is $+4R$. The gas diffusivities are D_1 and D_2, while Δn_1 and Δn_2 are the Ni and CO population changes from their far-field values. If we convert populations to pressures, we arrive at equations which must be solved self-consistently:

$$p_1 = p_{1\infty} - 5.35 \times 10^{10} exp\{-T_0/T_c\} \frac{\rho T_r}{D_1} f(p_1, p_2, T_c) \quad Torr \tag{21}$$

$$p_2 = 4 \frac{D_1}{D_2} (p_{1\infty} - p_1) \quad Torr \tag{22}$$

where $p_{1\infty}$ is the pressure far from the laser beam focal spot in Torr, and other variables have units as noted above.

The effects of diffusion are illustrated in Figure 1 for a 2 μm radius laser spot. We assume that the gas was at $T_r = 300°K$, not at T_c. For D_1 and D_2, we assume a 1 atm He buffer gas background, a common choice in our early experiments. Using the method of[R11], we obtain

$$D_1 = 0.23\ cm^2/sec; \quad D_2 = 0.93\ cm^2/sec \tag{23}$$

The inaccuracy in using (15) at low laser beam power levels is due to neglecting $f(p_{1\infty}, 0, T_c)$. Of more fundamental interest are the high power asymptotic results. This diffusion-limited

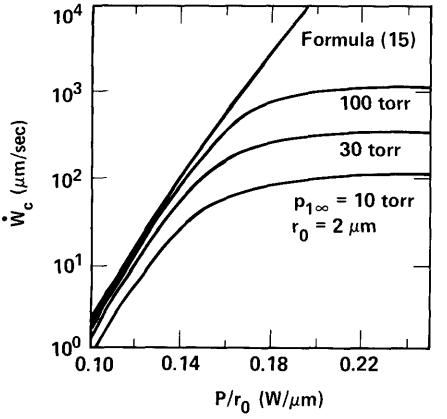

Figure 1 - Calculated Ni growth rate on Si substrate. The three right-most curves assume $r_0 = 2\ \mu m$.

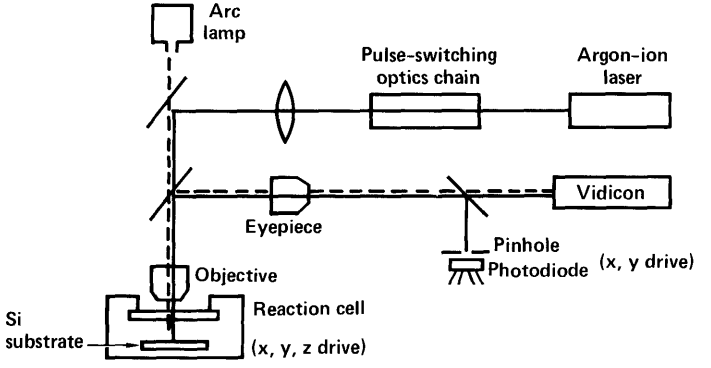

Figure 2 - Experimental arrangement for laser-pyrolytic deposition of metal microstructures.

rate is

$$R \lesssim \frac{2}{\sqrt{\pi}} \frac{D_1}{\rho} n_{1\infty} \tag{24}$$

Expressed in terms of metal-bearing gas pressure and growth rate of metal thickness, it is

$$\dot{W}_c \lesssim 9.1 \times 10^{-4} p_{1\infty}/\rho \quad \mu m/sec, \tag{25}$$

where $p_{1\infty}$ is in Torr and ρ is in cm. This limit is set by gas transport to the laser-heated spot on the surface; other factors enter only weakly through the radius of the metal spot, ρ. Small spot sizes and high partial pressures of $Ni(CO)_4$ are desirable in order to realize high metal trace growth rates. Fortunately, this is the regime of most interest to us.

This analysis assumes that the laser spot is being scanned "relatively slowly" over the substrate—$v \lesssim 500$ cm/sec—and that deposition is taking place onto Si. Obviously, most of the Ni metal deposition occurs on top of existing Ni. Since only a thin metallic layer ($\lesssim 0.01$ μm) is necessary to dominate reflectivity and absorption of laser light, we can assume that the entire laser spot sees the Ni reflectivity, $\Re_N$. Making the reasonable assumption that heat absorbed by the Ni transports primarily downward with little lateral conduction, then our analysis of the local Si temperature remains applicable for thin Ni layers, save for using $\Re_N$ in place of $\Re_S$. Using $\Re_N = 0.62$, the abscissa variable in Figure 1 now becomes $0.63P/r_0$. But our T_c is at the Si surface; the Ni surface is at a higher temperature and thus conducts the incident power down into the Si substrate. We can obtain a thickness limitation on the deposited metal film at which point the Ni starts to melt on its upper, laser-irradiated surface:

$$W_M = \frac{\pi r_0^2 K_N}{P(1-\Re_N)}(T_{mp} - T_c) \quad cm \tag{26}$$

Here T_{mp} is the Ni melting point of $1728°K$, K_N is its thermal conductivity of 0.7 $W/cm/°K$, and T_c is found from (14), using a value of $\Re_N$ of 0.62. As an example, consider a r_0 laser spot radius of 2 μm with a 0.6 watt incident laser beam power. We find that W_M in this case is 4.0 μm. This deposit thickness is attained quickly: a side effect of the large thermal gradient in the Ni is to drive the deposition process to the diffusion growth limit, so using (25) and (26),we find that melting occurs in a time t_M

$$t_M = 6.4 \times 10^7 (\frac{\rho}{r_0}) r_0^3 \frac{T_{mp} - T_c}{P p_{1\infty}} \quad sec \tag{27}$$

For 10 Torr $Ni(CO)_4$, $t_M = 34$ msec for the conditions just stated.

Dwelling at a location for longer than this time will cause melting of the top surface of the Ni. If the molten Ni spreads out, the line width of the metal trace being laid down will grow; if it doesn't have time to spread then, as more Ni is deposited, further temperature rise occurs, which can culminate in vaporization and spattering of superheated liquid Ni.

As a result, a single pass *minimum* scan rate V_{min} which just avoids melting under the stated conditions is

$$V_{min} \gtrsim 2\rho/t_M = 3.1 \times 10^{-8} \frac{P p_{1\infty}}{r_0^2 (T_{mp} - T_c)} \; cm/sec \tag{28}$$

EXPERIMENTAL STUDY

Description of Apparatus

Polished n-type silicon targets, typically oriented in [100] with 30 Ω-cm conductivity, were suitably cleaned and placed in a reaction cell having a sapphire entrance window. The cell was filled with the desired partial pressures of buffer gas and metal alkyl or carbonyl, and then irradiated by an argon-ion laser ($\lambda = 0.5145\ \mu m$) focused by one of two microscope objectives (10X, NA = 0.25; 36X, NA = 0.50).

Desired metal patterns (frequently lines) were created by moving the reaction cell with an x-y table stepper drive (1 μm steps; 1500 $\mu m/sec$ maximum speed), and by amplitude modulating the argon-ion laser beam by an optics chain which often included a half-wave plate followed by an electro-optics switch that was sandwiched between two Glan-Thompson prisms. During the course of each run, the laser patterns on the substrate and the deposited metal features were viewed through a microscope via a vidicon outputting to a color monitor. Laser beam profiles on the substrate were measured using a pinhole-photodiode arrangement mounted on a calibrated x-y drive located after the microscope. The samples were analyzed using optical and scanning electron microscopy (the latter with X-ray fluorescence capability) and stylus profilometry.

Results

Operating with present experimental conditions of $\sim$ 10 Torr of metal alkyl or carbonyl and ~ 0.4 W of 0.5145 μm radiation focused to $r_0 = 2-3\ \mu m$ on the Si surface, we observed rapid and localized deposition of Zn, Al and Ni from $Zn(CH_3)_2$, $Al(CH_3)_3$ and $Ni(CO)_4$. For scanning rates of $\sim 400\ \mu m/sec$, 2–6 μm wide and 0.2–10 μm high metallic lines were obtained in ~ 4 sweeps. The aluminum lines possessed a $\sim 0.5-2\ \mu m$ diameter puffy, quasi-periodic substructure, in part due to the discrete stepping translation of the wafer, while the nickel substructure consisted of close-packed quasi-spherical beads of $\sim 0.5-4\ \mu m$ diameter. At high laser power levels, the line deposited of each metal contained a smooth-surfaced central axial depression due to melting and compaction of the beads within the depression, as discussed above. As was particularly evident in the Ni and Zn studies, there was significant vaporization of metal from this central valley and consequential prenucleation of the nearby substrate surface when high laser powers were employed.

Figure 3 demonstrates that the thickness of the deposited Ni strip is linear with the number of sweeps and with the dwell time per 1 μm stepper jump, as predicted by our theory. Figure 4 shows preliminary data concerning the height of the deposited Ni line versus laser power applied to the target area. These runs were performed with a gas mixture consisting of 11 Torr $Ni(CO)_4$ plus 700 Torr He. These data indicate that Ni was deposited at a rate of $\sim 100\ \mu m/sec$ at higher laser power, in agreement with the theoretical prediction of Eq. (25) and Figure 1.

Variations in height within a given metal line and between different lines drawn under similar conditions are attributed to the nature of nucleation on the surface. At lower power levels, the method of surface preparation (various methods of cleaning polished Si surfaces covered by its native oxide, including cleaning and stripping away the SiO_2) greatly affected the production of nucleation sites. Prenucleation due to boiling of metal from nearby nickel lines was observed to greatly lower the nucleation threshold for subsequent low laser power pyrolytic metal deposition runs. Nucleation effects are expected to be of much less importance in planned work involving substrate temperatures raised to far above threshold temperatures for sub-microsecond periods.

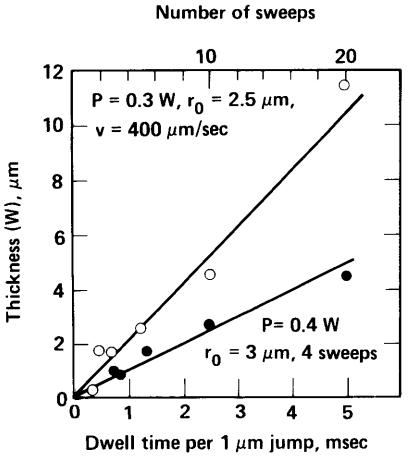

Figure 3 - Temporal dependence of nickel line deposition on silicon by laser pyrolysis (see text).

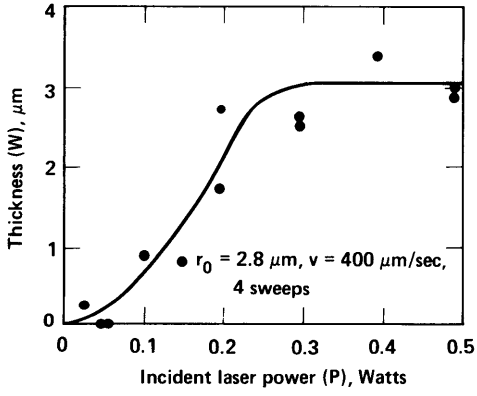

Figure 4 - Laser power dependence of pyrolytic deposition of nickel lines on silicon substrate (see text).

CONCLUSIONS

In this paper, we have reported a means for generating lines of metal suitable for use in ultra-large scale integrated (ULSI) circuits at rates which correspond to creating such circuits on times scales of a day. The best example of this approach involves the decomposition of metal, *e.g.*, nickel or iron, carbonyl positioned above the (typically semiconductor) surface of interest at mass transport-limited rates, with the pyrolytic deposition of the metal being energized and localized by transiently heating the surface with a focussed visible laser beam of suitable power level.

The first-principles theory which we have presented is quantitatively predictive of the preliminary experimental results which we have obtained with respect to all measured aspects of metal deposition. It asserts that metal depth build-up rates of the order of centimeters per second can be attained with the use of nickel and iron carbonyls, with somewhat lower rates being attainable for the carbonyls of other metals of interest, such as molybdenum and tungsten.

Sweeping (or otherwise time-modulating) a micron-scale laser beam spot relative to a location being metallized on a time scale of the order of 10 nanoseconds is predicted to be sufficient to intrinsically confine the deposition to within a 1 micron spot diameter on a silicon substrate, moreover very crisply, due to the exponential dependence of the deposition rate with surface temperature over the range of interest. Substrates of lower thermal diffusivity (e.g., silica) are tolerant of more prolonged exposure before 'thermal transport blurring' of the laser beam spot will ensue.

Our present experimental results include creation of micron-scale metal lines at deposition rates of 0.1 millimeter thickness per second with argon-ion laser beam powers in the range 0.3-0.6 W incident on the silicon substrate with beam spot sweep rates of more than 500 microns per second.

At multi-watt incident laser beam power levels and saturated carbonyl pressure above the substrate, our experimentally validated theory predicts that nickel/iron lines with micron-scale widths and thicknesses of several tenths of a micron can be deposited on a substrate of choice at a sweep rate of 10 cm/sec. This is quite adequate for computer-driven creation of ULSI circuits at interestingly high rates.

ACKNOWLEDGMENTS

The authors would like to express their gratitude to Dr. Richard Osgood for useful discussions during the course of this work, to James Atkins, Donald Duerre, Mark Garrett, Fred Mitlitsky and Elon Ormsby for their expert technical assistance in the experimental aspects of this study, and to Christine Ghinazzi for assistance in preparing this paper for publication.

REFERENCES

[R1] D. J. Ehrlich, R. M. Osgood, Jr. and T. F. Deutsch, IEEE J. Quant. Electron. **QE-16**, 1233 (1980).

[R2] D. J. Ehrlich, R. M. Osgood, Jr. and T. F. Deutsch, J. Electrochem. Soc. **128**, 2039 (1981).

[R3] R. Solanki, P. K. Boyer, J. E. Mahan and G. J. Collins, Appl. Phys. Lett. **38**, 572 (1981).

[R4] Y. Rytz-Froidevaux, R. P. Salathe and H. H. Gilgen, Phys. Lett. **84A**, 216 (1981).

[R5] S. D. Allen, J. Appl. Phys. **52**, 6501 (1981).

[R6] R. S. Berg and D. M. Mattox, "Proceedings of the Fourth International Conference on Chemical Vapor Deposition", edited by F. A. Glaski (Am. Nucl. Soc., Hindsdale, Illinois, 1973), p. 196.

[R7] H. E. Carlton and J. H. Oxley, A.I.C.L.E. Journal **12**, 86 (1967).

[R8] W. M. Goldberger and D. F. Othmer, IECPDE **2**, 202 (1963).

[R9] J. E. Moody and R. H. Hendel, J. Appl. Phys., **53**, 4364 (1982).

[R10] Y. I. Nissim, A. Lietoila, R. B. Gold and J. F. Gibbons, J. Appl. Phys., **51**, 274 (1980).

[R11] J. O. Hirschfelder, C. F. Curtiss and R. B. Bird, *Molecular Theory of Gases and Liquids* (John Wiley and Sons, New York, 1954) p. 14.